WSS/CI 98S-19

Comparison of CO Measurements by Raman Scattering and Two-Photon LIF in Laminar and Turbulent Methane Flames

R. S. Barlow and J. H. Frank
Combustion Research Facility
Sandia National Laboratories
Livermore, CA 94551-0969

G. J. Fiechtner
Innovative Scientific Solutions, Inc.
Dayton, OH 45440-3638

Presented at the 1998 Spring Meeting of the
Western States Section/The Combustion Institute
Sandia National Laboratories, Berkeley, CA, March 23-24, 1998


Sandia National Laboratories

COMPARISON OF CO MEASUREMENTS BY RAMAN SCATTERING AND TWO-PHOTON LIF IN LAMINAR AND TURBULENT METHANE FLAMES

R. S. BARLOW, J. H. FRANK
Combustion Research Facility
Sandia National Laboratories
Livermore, CA 94551-0969
barlow@ca.sandia.gov

and

G. J. FIECHTNER
Innovative Scientific Solutions, Inc.
Dayton, OH 45440-3638

ABSTRACT

Simultaneous measurements of CO concentration by Raman scattering and two-photon laser-induced fluorescence (LIF) are compared in several flames of methane and natural gas. The CO-LIF technique is shown to be much less affected than the Raman technique by interferences due to fluorescence from soot precursors that occur in hydrocarbon diffusion flames. The CO-LIF technique is also shown to have better precision and therefore to have a greater potential for extension to measurements of low CO concentrations in turbulent lean premixed methane flames.

INTRODUCTION

Single-shot, spatially-resolved measurements of CO concentration are needed in several areas of combustion research and development involving hydrocarbon fuels. With regard to fundamental research on turbulent combustion processes, such measurements are needed because CO is an important combustion intermediate. Accurate measurements of CO concentration in turbulent flames can allow detailed evaluations of reduced chemical mechanisms and computational submodels for the interactions of fluid dynamics and chemistry. These issues of combustion fundamentals and model validation must be addressed as quantitatively as possible in both nonpremixed and premixed combustion. With regard to practical combustion applications, such as power generation by stationary gas turbines, CO is an important pollutant that must be controlled. CO concentration measurements in turbulent lean premixed natural gas flames may provide a better understanding of the processes that affect CO emissions, and this may lead to better predictive design tools.

Spontaneous Raman scattering and two-photon laser-induced fluorescence have both been used to measure CO in hydrocarbon flames. Raman scattering measurements in the blue regions piloted jet flames of undiluted methane were reported by Masri et al. [1-3]. Their study made use of a flashlamp-pumped dye laser operated at 532 nm, and they reported significant interference on the CO Raman scattering measurements due to laser-excited fluorescence of hydrocarbons [4]. Experiments on several other pilot- and bluff-body-stabilized jet flames have been conducted as part of a long-term collaboration between Sandia and Sydney University, and this work has been reviewed by Masri et al. [5]. Correa et al. [6] have also reported multiscalar Raman scattering measurements in a bluff-body methane flame, using a flashlamp-pumped dye laser at 488 nm. They also reported significant fluorescence interferences on the CO-Raman measurements, and they commented on the "need for better measurements of CO than Raman spectroscopy can provide." More recently, Bergmann et al. [7] have reported Raman measurements in jet flames of $CH_4/H_2/N_2$, also using a flashlamp-pumped dye laser at 488 nm. The addition of H_2 and N_2 served to reduce but not eliminate the fluorescence interferences.

The hydrocarbon fluorescence interferences affect the Raman scattering measurements of several species, but CO measurements are strongly affected due to the relatively low number densities of CO in methane flames. When 532 nm light is used, much of the interference is from C_2 fluorescence, which has a band that happens to align with the CO Raman detection wavelength. Consequently, the measurement uncertainties in reported CO concentrations have been relatively large, and this has lead to controversy regarding the levels of CO in turbulent nonpremixed methane flames. CO levels measured in experiments on undiluted methane flames were higher than those calculated for steady strained laminar flames or predicted by pdf models [6,8]. CO levels reported in methane flames having N_2 or air dilution in the fuel jet have been reasonable consistent with laminar flame calculations, and it has not been clear whether the high measured CO levels in undiluted methane flames are real effects of turbulence-chemistry interactions or artifacts of the measurement technique.

Multiscalar Raman scattering measurements, including CO, have also been performed in laminar [9] and turbulent premixed methane-air flames [10,11,12]. In such flames there are minor fluorescence interferences when the probe volume intersects the thin flame front. However, CO-Raman measurements in the post-flame products have been free of interferences. The problem for Raman scattering in lean premixed methane flames is that the CO concentrations and the resulting Raman signals are too low for useful single-shot measurements with available laser energies.

These problems of fluorescence interference in nonpremixed flames and low signals in lean premixed flames have motivated that addition of CO two-photon LIF to the combine multiscalar diagnostic system in the Turbulent Diffusion Flame (TDF) lab at Sandia. Several experiments involving CO-LIF measurements in flames have been reported in the literature [13-17]. These have demonstrated the potential utility of this diagnostic technique, but have also highlighted issues of signal dependence on laser power, temperature, and collisional quenching that must be considered when interpreting the measurements. Fiechtner et al. [12] have recently conducted detailed investigation of some of these issues. The present paper compares CO measurements

performed simultaneously using Raman scattering and two-photon LIF. The optical configurations and diagnostic strategies are described, and results from several types of methane (and natural gas) flames are presented.

EXPERIMENTAL METHODS

Experiments were conducted in the TDF lab at Sandia. Simultaneous point measurements of multiple scalars are obtained using the combination of Rayleigh scattering, Raman scattering, and laser-induced fluorescence. The flow facility, diagnostic systems, and calibration procedures have been reported previously [9,18,19]. Here we provide a more complete description of certain aspects of the experiment to document improvements to the diagnostic systems and to describe the strategies for the CO-Raman and CO-LIF measurements.

Raman/Rayleigh Optical System, Calibrations, and Data Reduction

Figure 1 shows the optical configuration of the Raman/Rayleigh system. The frequency doubled beams from two pulsed Nd:YAG lasers (10 Hz, 532 nm, ~1 J combined energy per pulse) were temporally stretched to avoid gas breakdown in the probe volume. The pulse stretcher employed two delay loops of approximately 18 ns and 9 ns, with each loop constructed of a beam splitter (38%R @ 532-nm P-polarized, AR coated on the back side) and mirrors aligned to place the delayed pulses on the same axis as the initial beam. The stretched beams were focused into the probe volume by a 1.5-m fl lens, recollimated by a 0.5-m fl lens on the far side of the test section, and folded back by a prism for a second pass through the probe volume to effectively double the Raman and Rayleigh signals. Pulse energies were measured using two pyroelectric joule meters. Alignment of the pulse stretcher and the monitoring of that alignment during experiments was accomplished by splitting off a small fraction of the beam after the focusing lens and projecting the focal volume onto a low-cost video CCD chip.

Scattered light was collected by a symmetric six-element achromat and relayed by a 50-mm-fl, f/1.2 camera lens. A holographic edge filter reflected the 532-nm Rayleigh scattered light to a photomultiplier tube (PMT) located outside the Raman polychromator. Raman scattered light was focused onto the entrance slit of a 3/4-m SPEX 1801 spectrometer with the image of the probe beam aligned perpendicular to slit. A 1/2-waveplate located inside the spectrometer rotated the polarization to allow optimal efficiency of the 1800 line/mm holographic grating. An array of PMT's (Hamamatsu R1477) detected Raman scattered light from the major species, and signals were digitized using a 16-channel, 12-bit charge integrator (Phillips Scientific 7166) with a 600-ns gate width. PMT sockets were custom wired, and each Raman/Rayleigh channel was tested to insure linear response over the range of signals observed in these experiments.

Temperature-dependent calibration functions for each of the Raman channels were developed from an extensive series of measurements in the flow exiting an electric heater (up to about 900K) and in flat flames above a Hencken burner. The Hencken burner was constructed of small fuel tubes arrayed in a stainless steel honeycomb matrix, such that each fuel tube is surrounded by six air flow passages. When properly operated, the burner is nearly adiabatic because the burner is cooled mainly by the flowing reactants rather than by radiation from the burner surface. Calibration measurements were made in the post-flame gases 3 cm above the burner surface. Calibration flames included H_2-air, H_2/O_2-air, H_2/N_2-air, CO/H_2-air, $CO/H_2/O_2$-air, $CO/H_2/N_2$-air, and CH_4-air mixtures. Hydrogen and CO flames were operated in a nonpremixed mode on the Hencken burner, allowing wide ranges in the overall equivalence ratio. CH_4-air flames were operated in a premixed mode over a more limited range of equivalence ratio due to the lower flame speed of methane.

In each calibration flow or flame the temperature was determined from Rayleigh scattering. Rayleigh cross sections for the flames were determined from adiabatic equilibrium calculations based on the calibrated flow rates. Species concentrations were then determined from an equilibrium calculation at the measured Rayleigh temperature. For the CO/H_2-air and CH_4-air flames, where CO_2 radiation was an important loss mechanism, the measured Rayleigh

temperatures were approximately 50K below adiabatic equilibrium. The H_2-air flame radiated less, and the assumption of adiabatic equilibrium concentrations of the major species was appropriate, provided the reactant flow rates were sufficiently high (we have used at least 90 slm total flow for a 50-mm diameter burner).

The temperature-dependent response of each Raman channel was fitted by a polynomial of up to 6th order. There was crosstalk among some of the Raman species, which had to be calibrated before some of the Raman calibrations could be generated. For example, the N_2 Raman spectrum overlapped the CO Raman detector. The generation of calibration functions proceeded in the following order. Heater data and H_2 flame data were used for Raman calibrations of N_2, O_2, H_2, and H_2O, plus the crosstalk calibrations of $N_2 \rightarrow CO$, $O_2 \rightarrow CO_2$, $H_2 \rightarrow CO_2$, $H_2 \rightarrow O_2$, $H_2 \rightarrow CO$, and $H_2O \rightarrow H_2$. The calibration for the crosstalk of N_2 onto CO was highly repeatable and the residual error in CO was typically below a mole fraction of 10^{-4}. Raman calibrations functions for CO and CO_2 and crosstalk calibrations for $CO_2 \rightarrow O_2$ were based on heater data and data from CO/H_2 and CH_4 flat flames. The CO-Raman response is relatively insensitive to temperature. However, the calibration between about 900 and 1800 K is based on interpolation rather than direct calibration, so the estimated uncertainty is greater in this temperature range.

LIF Optical Systems and the Strategy for CO Two-Photon LIF Measurements

The optical configuration of the LIF systems for OH, NO, and CO are shown in Fig. 2. Diagnostic strategies for OH and NO have been described previously [9,18,19] and are not discussed here. The CO LIF system included a Nd:YAG-pumped dye laser combination with wavelength extension (Spectra Physics DCR-2A, PDL-2, WEX). A double and mix scheme was used to generate ~0.7 mJ/pulse in the test section at 230.1 nm. (Energy was limited by the need for several reflections to direct the beam from the first floor of the lab up to the optical table on the second floor.) Energy was measured using a photodiode and referenced to a joulemeter reading in the test section. The Nd:YAG laser was seeded, providing a typical rms fluctuation of laser energy in the probe volume of between 3.1 and 3.5%. Laser wavelength was adjusted based on the fluorescence from a room-temperature cell having a low flow of 50% N_2, 45% He, and 5% CO. The peak of the $B^1\Sigma(v'=0) \leftarrow\leftarrow X^1\Pi(v''=0)$ band excitation scan from the cold cell was used as a wavelength reference, and the laser was tuned by a fixed amount to a position corresponding to a relatively flat region in the flame spectrum. The laser ($\Delta\nu \sim 0.6$ cm^{-1}) overlaps several CO lines. The CO-LIF emission from the $B^1\Sigma(v'=0) \rightarrow A^1\Pi(v''=0)$ band was detected using a PMT with two bandpass filters (10-nm and 25-nm bandwidths) centered at 484 nm. The combination of filters was used to protect the PMT from the large 532-nm Rayleigh-scattering signal, and we note that other strategies might allow for a lower CO detection limit. For the experiments described here we did not attempt to optimize the sensitivity of the system.

The loss mechanisms from the CO excited state include collisional quenching and ionization by a third photon. In the present experiments the 230-nm beam was focused, and the measured energy dependence of the fluorescence signal was close to unity (less than 1.3). Suggesting that ionization may have been the dominant loss mechanism. However, experiments and analysis indicate that the measurements may not be completely independent of quenching. There is not sufficient data on the spectroscopic properties of CO and collisional quenching cross sections to allow shot-to-shot corrections for these effects. Therefore, we have used calibration and data reduction strategies for the CO-LIF measurements that is similar to that for the Raman measurements. A temperature dependent calibration function was generated based on measurements up to 900 K above the electric heater and between about 1900 and 2300K in the CO/H_2 and CH_4 flat flames. The shape of this calibration curve in the interpolated temperature range and through flame temperatures is based on a calculation by Mike Di Rosa [20] of the two-photon absorption cross section. The laser energy fluctuations were small enough and average power was stable enough to neglect the non-unity power dependence of the CO fluorescence, and signals were simply normalized by laser energy. This simplification did not significantly effect the fluctuations (noise) in CO-LIF measurements performed in steady, uniform calibration flows and flames.

COMPARISON OF SIMULTANEOUS CO MEASUREMENTS

Simultaneous Raman and LIF measurements of CO concentration are compared in four types of flames: i) premixed methane-air flat flames, ii) laminar methane-air jets flames, iii) a pilot-stabilized turbulent methane-air jet flame, and iv) a pilot-stabilized turbulent jet flame of natural gas.

Premixed CH_4-air Flat Flames

Figure 3 shows results of Raman/Rayleigh/LIF measurements in a series of premixed methane-air flat flames. These flames were stabilized on a 50-mm-diameter Hencken burner operated in a premixed mode, with premixed reactants flowing through the "air-side" of the burner. Flow rates were set such that most of the cell structure of the premixed flame is actually lifted above the surface to keep the burner relatively cool. Measurements were made in the post-flame products 3 cm above the burner. This series of methane-air flames was part of the complete Raman calibration series. However, the calibration curves for CO-Raman response and $N_2 \rightarrow CO$ crosstalk that were used in reducing these data were based primarily on the heated flows and the H_2 and CO/H_2 flames. The symbols in Fig. 3 show the average temperature and the concentrations of selected species. The solid curve for temperature represents an average over several such calibrations sets of the measured Rayleigh temperature. This Rayleigh temperature curve is about 50 K below the adiabatic equilibrium curve (not shown). The solid curves for species correspond to the equilibrium concentrations calculated at this averaged Rayleigh temperature.

Here, the CO-Raman and CO-LIF calibrations were both tuned to match (on average) the CO/H_2 calibration flame conditions for concentrations above 0.0002 mol/l. The two CO measurements are in reasonably good agreement in these methane flames, except at low concentrations, where there is a consistent offset of the CO-LIF results above the CO-Raman results. This offset may be due to photodissociation of CO_2, which has been reported by Nefedov et al. [21]. This interference results in an error of approximately 2×10^{-5} mol/l at a temperature of about 2100 K and a CO_2 concentration of about 5×10^{-4} mol/l. This is a relatively small error compared to the peak concentrations of CO in methane diffusion flames, and we have not corrected for it in the present work. It is important to note that measurements of the low CO concentrations that occur in lean premixed methane-air flames may require accurate corrections for this CO_2 interference, and further work is needed to quantify this effect.

The error bars in Fig. 3 correspond to rms fluctuations in the CO measurements. The CO-LIF measurements offer a clear advantage in this regard. The higher CO concentrations in this premixed series are comparable to the maximum concentrations in nonpremixed methane flames. In this upper range the LIF technique yields fluctuations about 2.5 times smaller than the Raman technique, as applied in this experiment. At low CO concentrations the LIF advantage is even greater because the random error on in the CO-Raman measurements becomes dominated by shot noise in the crosstalk from N_2 onto the CO-Raman PMT.

Laminar CH_4-air Jet Flame

Measurements in laminar CH_4-air diffusion flames provide an illustration the problem of hydrocarbon fluorescence interferences in CO-Raman measurements and of the methods used to correct for them. The interferences come from a variety of hydrocarbon species, including PAH and other soot precursors, that are formed on the fuel-rich side of hydrocarbon diffusion flames. The composition of this hydrocarbon soup and hence the intensity and spectrum of the interference depends on several factors, including fuel type, dilution, local scalar dissipation rate, local stoichiometry, and convective residence time up to the measurement location. When a 532-nm laser is used for the Raman measurements, the spectrum of the largest fluorescence interferences includes distinct C_2 fluorescence bands on top of a broad background. The approximate position of the C_2 bands relative to the vibrational Raman scattering spectrum is illustrated in Fig. 4. A

photomultiplier tube (F615) detects a portion of this C_2 fluorescence interference and this signal may be used to correct the Raman measurements in some situations as described below.

A scatter plot of the F615 signal versus mixture fraction measured across a radial profile in a laminar methane-air jet flame is shown in Fig. 5. The fuel-side composition was 25% CH_4 and 75% air. This partial premixing with air reduces the tendency to form soot, so that the flame is blue over most of its length. Scalar dissipation rates are sufficiently high, even in this laminar flame, that the rich premixed chemistry is negligibly slow, and the flame burns as a diffusion flame with a single reaction zone surrounding the stoichiometry value of the mixture fraction (F_{stoic}=0.351). The fluorescence interference is greatest for mixture fractions between 0.4 and 0.55. There is also a signal on the F615 channel due to Raman scattering from CH_4. This signal was calibrated as a function of temperature based on measurements in heated CH_4/N_2 flows and accounted for in the processing of the Raman data.

Figure 6 shows the temperature and selected species concentrations calculated for a laminar opposed-flow flame with a fuel-side composition of 25% CH_4 and 75% air and a strain parameter of a=100 s^{-1} (calculation provided by J.-Y. Chen). At this strain rate there is a single reaction zone and no significant premixed chemistry on the fuel-rich side. Starting from low levels on the lean side, the CO concentration rises sharply through the reaction zone and displays a broad peak of about 3.5×10^{-4} mol/l between 0.45 and 0.60 in mixture fraction. The location of this peak in CO concentration coincides with the largest fluorescence interferences. The effect of the interferences on Raman scattering measurements of CO is shown in Fig. 7. Here the results have been corrected for all the calibrated crosstalk between Raman species, but they have not been corrected for the fluorescence interference that lands on the CO Raman detector. In this laminar jet flame the apparent CO concentrations in the region of greatest interference are 3 to 5 times the true concentrations.

Figure 8 shows the correlation between the F615 signal and the excess signal on the CO-Raman PMT. This result suggests that a simple constant factor can be used to correct the CO-Raman concentrations. (Note that the most of the very rich data which are most affected by Raman crosstalk from CH_4 are not plotted in Fig. 8.) The effect of such a correction is shown in Fig. 9, which includes data from a separate set of measurements in the same type of air-diluted laminar jet flame. The corrected data (open symbols) are consistent with the CO concentrations given by the laminar flame calculations. However, the precision of the correction is not very satisfactory, and there remains significant scatter in CO concentration within the region of greatest interference.

The CO-LIF technique is much less affected by hydrocarbon fluorescence interferences. This is demonstrated by Fig 10, where the normalized CO-LIF signals from the same data set as in Fig. 7 (simultaneous Raman and LIF measurements) are plotted versus the mixture fraction. Also plotted are the corresponding signals from the CO-LIF channel from a radial profile taken with the laser tuned off of the CO resonance. The off-resonance signal is a small fraction of the CO fluorescence signal. An unanticipated benefit of the simultaneous Raman/Rayleigh/LIF measurements is that there is a reasonably good correlation between this off-resonance CO-LIF signal and the F615 signal. Figure 11 shows radial profiles in the laminar jet flame of the average off-resonance signal on the CO-LIF detector and the average F615 signal. Here the profiles have been scaled so that the peak values are equal. Note that the CH_4-Raman signal has not yet been subtracted from the F615 results. This correlation has allowed shot-to-shot corrections that remove more than half of the already small interference on the CO-LIF measurement that comes from hydrocarbon fluorescence.

Piloted CH_4 Jet Flames with Partial Air Premixing

Partial premixing of air with methane, as in the above laminar jet flame, creates flames that are "Raman friendly" in that the levels of soot and soot precursors are significantly reduced compared to those in flames on undiluted methane. Furthermore, the partial premixing yields a more robust flame that may be operated at higher jet velocities before strain-induced extinction becomes an issue. This translates to shorter residence times for the formation of higher hydrocarbons. It also translates to higher Reynolds numbers, which are useful for validation of

turbulent combustion models. We have recently completed a comprehensive investigation of piloted jet flames with the 25% CH_4 and 75% air mixture [22].

Figure 12 compares the conditional average mass fractions of CO measured simultaneously by Raman scattering and by two-photon LIF across a radial profile at an axial distance of 30 nozzle diameters from the base of a flame having a jet exit Reynolds number of 22,400 (d=7.2 mm, U_{jet}=49.6 m/s). Here, the CO-LIF data have been temperature corrected and corrected for the portion of the off-resonance signal that correlates with the F615 channel. The CO-Raman data have been corrected for interference, using the method described above, and for crosstalk from other Raman species. The region of hydrocarbon fluorescence interference is shaded in the figure, and one can see that the correction to the Raman measurements works well on average at the center of this region. However, the Raman results are undercorrected for mixture fractions between about 0.4 and 0.5, while they are over corrected for mixture fractions between 0.5 and 0.6. This results from the fact that the spectrum of the fluorescence interference depends on the local composition and temperature in the probe volume. The CO-Raman and CO-LIF results are in close agreement near the stoichiometric value of the mixture fraction, where direct calibrations are available for both techniques. The small offset of the CO-LIF above the CO-Raman, which may be due to photodissociation of CO_2, is evident in the fuel-lean portion of the graph. Results diverge somewhat in the richest end of the curves, and this may be due to incomplete correction of the Raman data for the effects of crosstalk from CH_4. Differences in the quenching rate between the heater calibration conditions and the rich flame conditions may also contribute to this divergence.

The conditional fluctuations of the two CO measurements are plotted as uncertainty bars in Fig. 12. The CO-LIF method yields lower conditional fluctuations, especially in the region of hydrocarbon fluorescence interference. Note that relative fluctuations in the CO-LIF measurements are greater in this piloted flame than in the premixed flat flames due to turbulent fluctuations in the instantaneous CO mass fraction.

Piloted Natural Gas Jet Flame

Flames of undiluted methane or natural gas are distinctly unfriendly to the Raman scattering technique because they tend to produce soot. Generally, Raman scattering measurements have only been attempted in the blue regions of such flames. Even in these blue regions the levels of soot precursors can be high enough to cause major problems for the Raman scattering technique. Figure 13 shows a scatter plot of the apparent CO concentration from Raman scattering measurements in a turbulent, piloted jet flame of natural gas. The piloted burner was developed at the Technical University of Delft [23] and was investigated at Sandia as part of a collaboration to develop experimental data sets for combustion model validation [24]. The fuel was natural gas with added N_2 to match the composition of Dutch natural gas (~14% N_2). The stoichiometric value of the mixture fraction in this flame was 0.071, as marked in the figure. Measurements in Fig. 13 were obtained across a radial profile at 25 mm from the nozzle, which is well below the location where soot becomes visible. Still, the largest interferences cause apparent concentrations that are 15 to 20 times the concentrations given by a strained laminar flame calculation (provided by P. Nooren). Figure 14 demonstrates that the correction scheme that worked reasonably well in the air-diluted methane flames is completely inadequate in this natural gas flame, and one must conclude that Raman scattering measurements of CO in this flame are useless.

In contrast, the simultaneous measurements of CO by LIF in this flame (Fig. 15) appear to work very nicely. These CO-LIF measurements have been corrected for interferences based on a correlation between the off-resonance signal and the F615 signal obtained in a separate measurement. The CO concentrations from the LIF measurements are slightly higher on average than the laminar calculation. However, these particular results are from an early stage in the process of data analysis, using a preliminary calibration for the CO-LIF, and one should not draw any quantitative conclusion regarding the effect of turbulence on CO concentrations from this figure.

SUMMARY

These comparisons of simultaneous measurements of CO concentration by Raman scattering and two-photon laser-induced fluorescence have demonstrated that the CO-LIF method is much less affected than the CO-Raman method by interferences due to fluorescence of hydrocarbons in methane and natural gas diffusion flames. The addition of the CO-LIF capability to the multiscalar point measurement system at Sandia has allowed a significant improvement in the precision and accuracy of CO measurements obtained in hydrocarbon diffusion flames.

There are indications from the literature and from the present data that photodissociation of CO_2 may interfere with two-photon LIF measurements of CO. This is not a significant problem for methane diffusion flames, and we have not attempted to correct for this interference in the present work. However, the extension of the CO-LIF measurements to the very low concentrations that occur in the CO burnout region of turbulent lean premixed methane-air flames will most likely require a more detailed consideration the CO_2 photodissociation issue.

The extension of these measurements to the burnout region of turbulent lean premixed flames may also require more detailed information on the spectroscopic properties and collisional quenching cross sections of CO. This is because it may not be practical or possible to produce reliable calibration flows for the CO-LIF method that cover the temperature range and quenching environment of interest in lean premixed combustion studies. Consequently, measurements may have to rely on calibrations such as those used in the present study, combined with corrections based upon detailed analysis of the fluorescence equation.

Acknowledgments

Work at Sandia was supported by the United States Department of Energy, Office of Basic Energy Sciences. CDC was supported by the AFOSR under Air Force Contract F33615-92-2202. This work has benefited from useful discussions with R. Faro and M. DI Rose. Special thanks to P. Nooren for bringing his "Kuwait oil fire" to the TDF lab.

REFERENCES

1. Masri, A. R., Bilger, R. W., Dibble, R. W., Combust. Flame 71:245-266 (1988).
2. Masri, A. R., Bilger, R. W., Dibble, R. W., Combust. Flame 73:261-277 (1988).
3. Masri, A. R., Bilger, R. W., Dibble, R. W., Combust. Flame 74:267-284 (1988).
4. Masri, A. R., Bilger, R. W., Dibble, R. W., Combust. Flame 68:109-119 (1987).
5. Masri, A. R., Dibble, R. W., and Barlow, R. S., *Pro. Energy Comb. Sci.* 22:307-362 (1996).
6. Correa, S. M., Gulati, A., and Pope, S. B., *Twenty-Fifth Symposium (International) on Combustion*, The Combustion Institute, Pittsburgh, PA, 1994, pp. 1167-1173.
7. Bergmann, V., Meier, W., Wolff, D., and Stricker, W., *Appl. Phys. B* (to appear).
8. Chen, J.-Y., Kollmann, W., and Dibble, R. W., *Comb. Sci. Tech.* 64:315-346 (1989).
9. Nguyen, Q. V., Dibble, R. W., Carter, C. D., Fiechtner, G. J., and Barlow, R. S., *Combust. Flame* 105:499-510 (1996).
10. Nandula, S. P., Pitz, R. W., Barlow, R. S., and Fiechtner, G. J., AIAA paper 96-0937 (1996).
11. Frank, J. H., and Barlow, R. S., "Simultaneous Rayleigh/Raman/LIF Measurements in Turbulent Premixed Methane-Air Flames," submitted to the 27th Combustion Symposium (1998).
12. Fiechtner, G. J., and Barlow, R. S., in preparation.
13. Alden, M., Wallin, S., and Wendt, W., *Appl. Phys. B* 33:205-208 (1984).
14. Seitzman, J. M., Haufmann, J., and Hanson, R. K., *Appl. Optics* 26:2892-2899 (1987).
15. Tjossem, P. J. H., and Smyth, K. C., *J. Chem. Phys.* 91:2041-2048 (1989).
16. Everest, D. A., Shaddix, C. R., and Smyth, K. C., *Twenty-Sixth Symposium (International) on Combustion*, The Combustion Institute, Pittsburgh, PA, 1996, pp. 1161-1169.

17. Mokhov, A. V., Levinsky, H. B., van der Meij, C. E., and Jacobs, R. A. A. M., *Appl. Optics* 34:7074-7082 (1995).
18. Barlow, R. S., and Carter, C. D., *Combust. Flame* 97:261-280 (1994); and *Combust. Flame* 104:288-299 (1996).
19. Barlow, R. S., Fiechtner, G. J., and Chen, J.-Y., *Twenty-Sixth Symposium (International) on Combustion*, The Combustion Institute, Pittsburgh, PA, 1996, pp. 2199-2205.
20. Di Rosa, M., Sandia National Laboratories, personal communication.
21. Nefedov, A. P., Sinel'shchikov, V. A., Usachev, A. D. and Zobnin A. V., *Appl. Optics* (to appear).
22. Barlow, R. S., and Frank, J. H., "Effects of Turbulence on Species Mass Fractions in Methane/Air Jet Flames," submitted to the 27th Combustion Symposium (1998).
23. Nooren, P. A., Wouters, H. A., Peeters, T. W. J., Roekaerts, D., Maas, U., and Schmidt, D., *Combustion Theory and Modeling* 1:79-96 (1997).
24. The Delft/Sandia collaboration was established as part of the International Workshop on Measurement and Computation of Turbulent Nonpremixed Flames, www.ca.sandia.gov/tdf/Workshop.html. These experiments are part of the thesis work of P. Nooren.

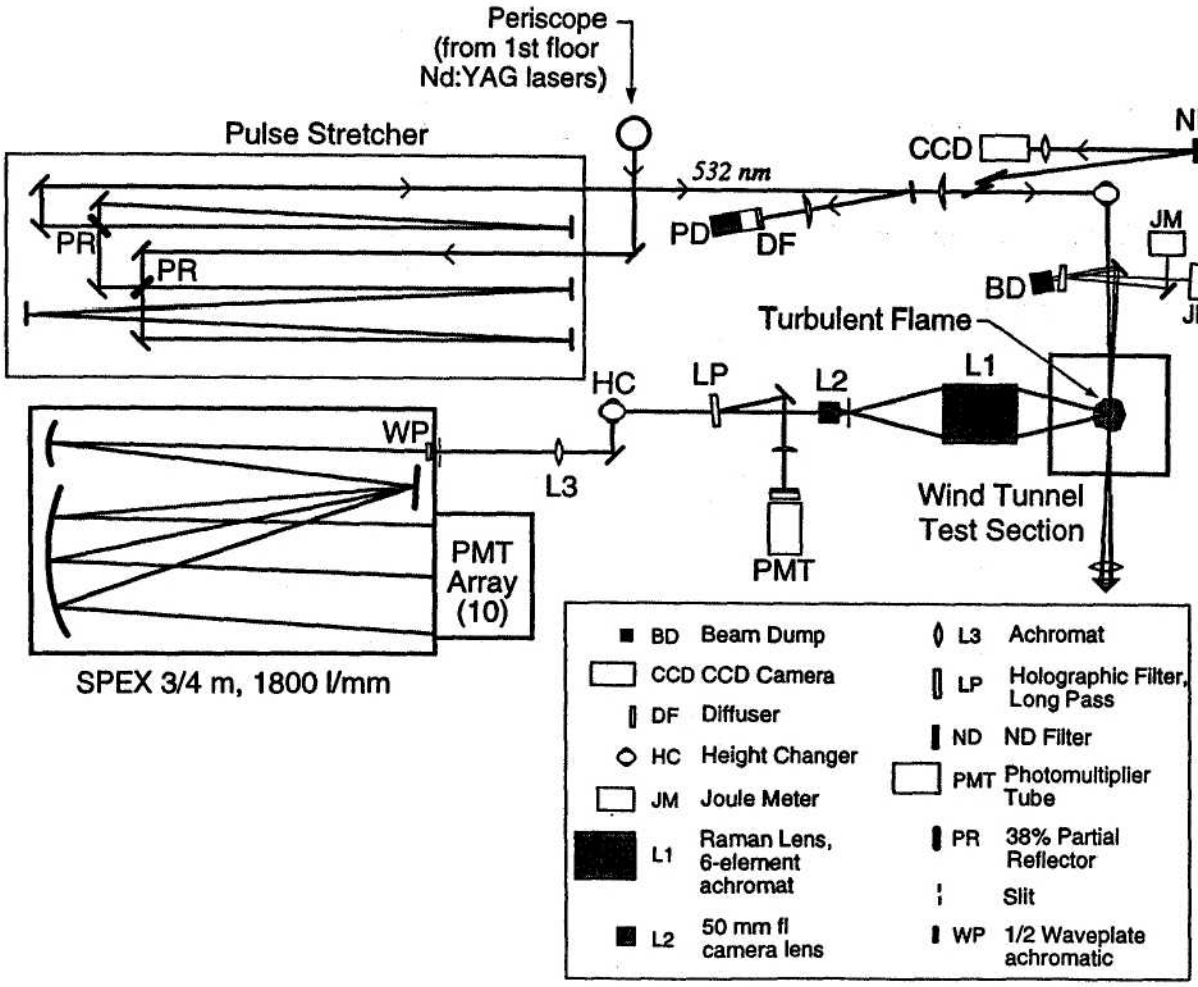

Fig. 1. Optical configuration of the Raman/Rayleigh system.

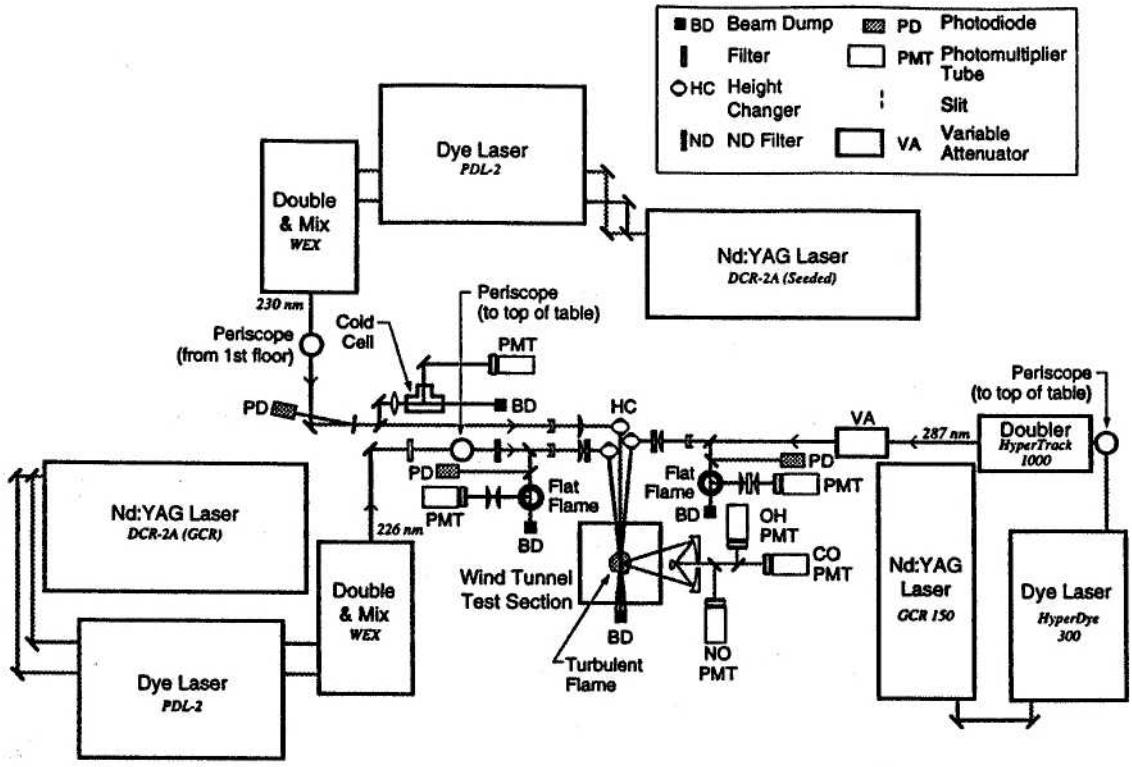

Fig. 2. Optical configuration of the three LIF systems for measurements of CO, OH, and NO.

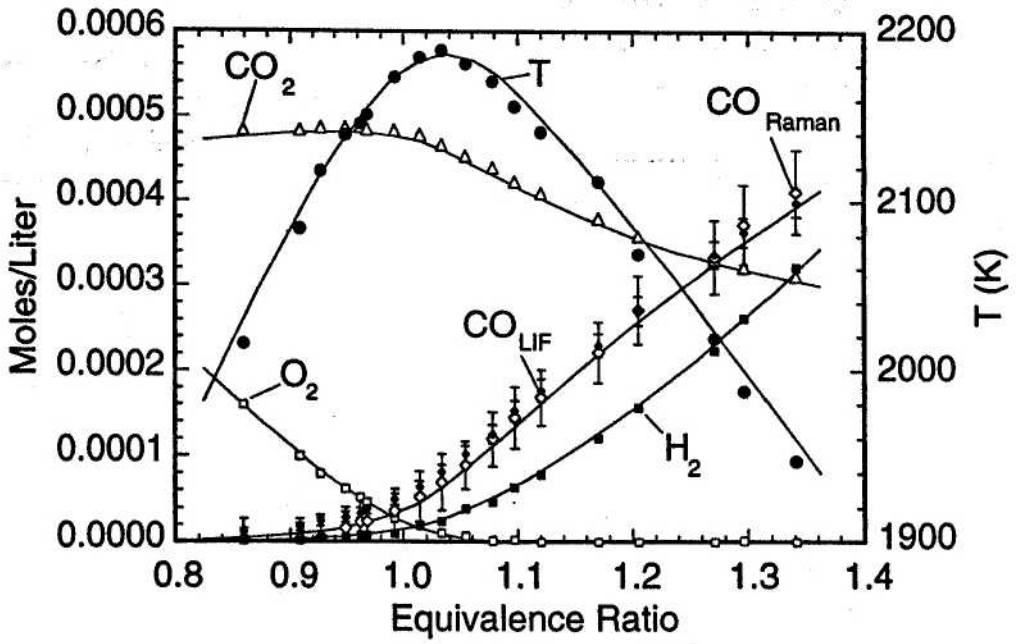

Fig. 3. Temperature and concentration measurements above a series of premixed methane-air flat flames stabilized on the Hencken burner. Solid lines represent non-adiabatic equilibrium conditions. Uncertainty bars on the CO measurements represent rms fluctuations ($\pm\sigma$) in the processed concentrations.

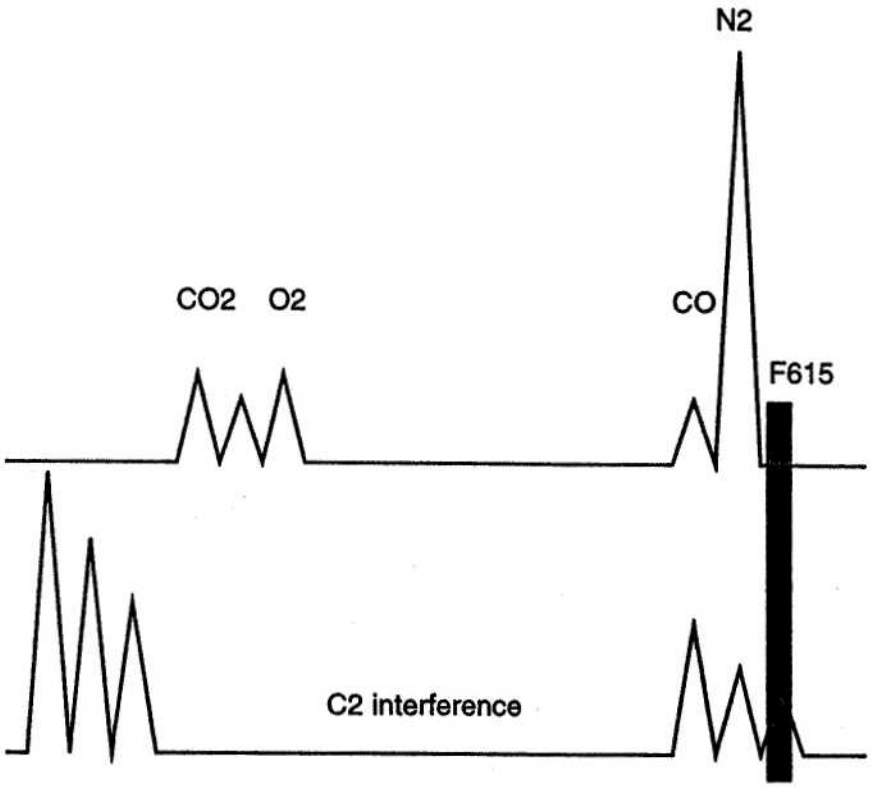

Fig. 4. Relative locations of C_2 Swan bands, vibrational Raman scattering bands (532-nm laser), and the F615 PMT used to monitor hydrocarbon fluorescence interference.

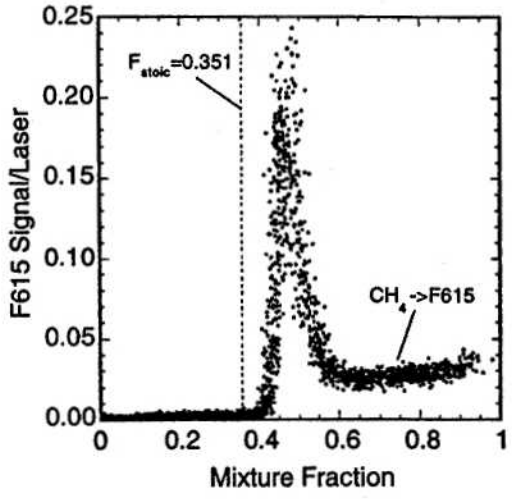

Fig. 5. Scatter plot of F615 signal versus mixture fraction in a laminar methane-air jet flame.

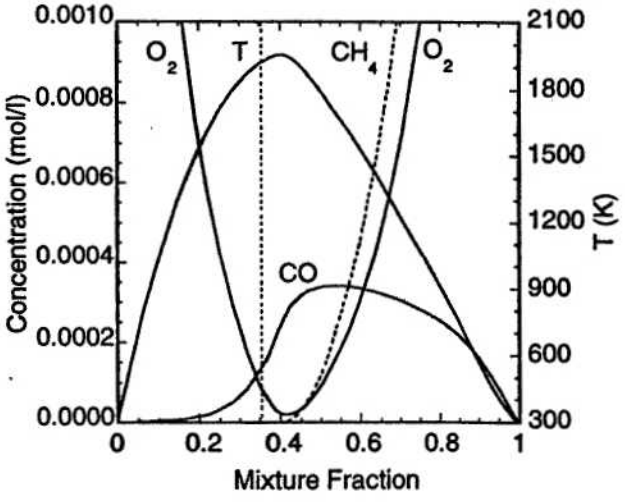

Fig. 6. Calculated temperature and species concentrations a laminar opposed-flow flame at a strain parameter of a=100 s^{-1}.

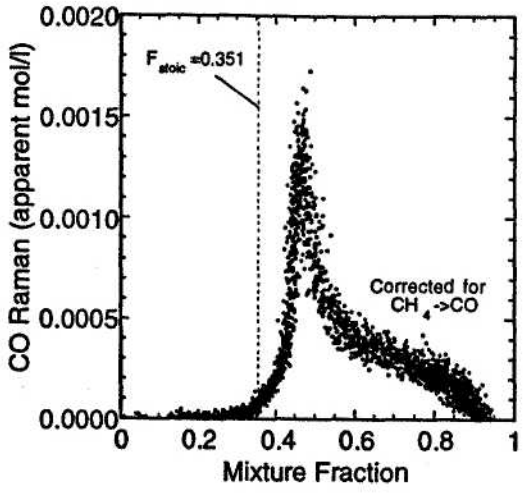

Fig. 7. Scatter plot of apparent CO concentration from Raman scattering measurements in the laminar methane-air jet flame.

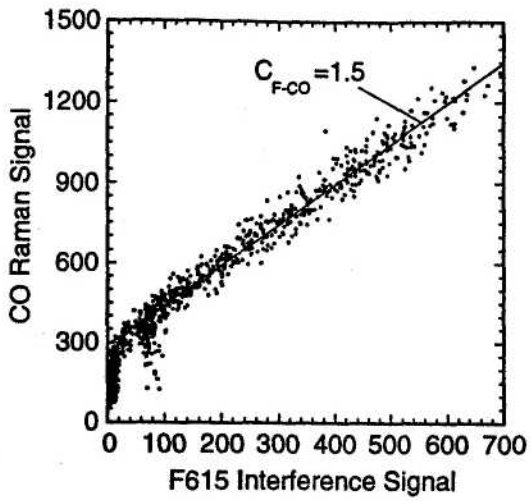

Fig. 8. Correlation between the F615 signal and the excess signal on the CO-Raman channel.

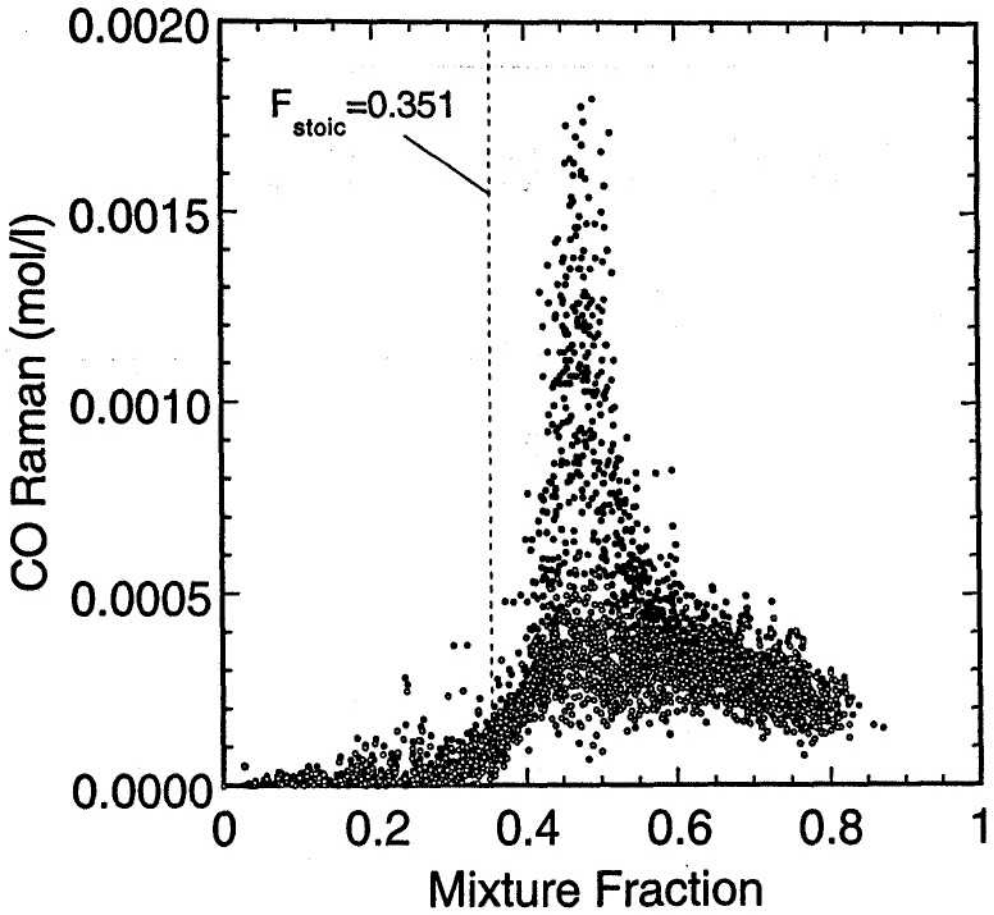

Fig. 9. Comparison of uncorrected (filled symbols) and corrected (open symbols) CO concentration results for a laminar methane-air jet flame.

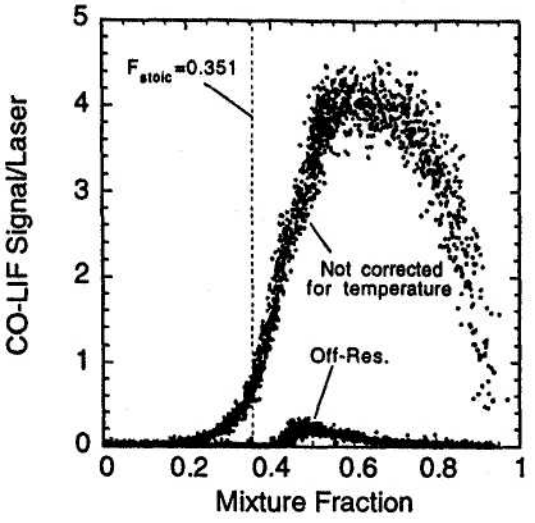

Fig. 10 Relative magnitudes of on- and off-resonance CO-LIF signals measured in the laminar methane-air jet flame.

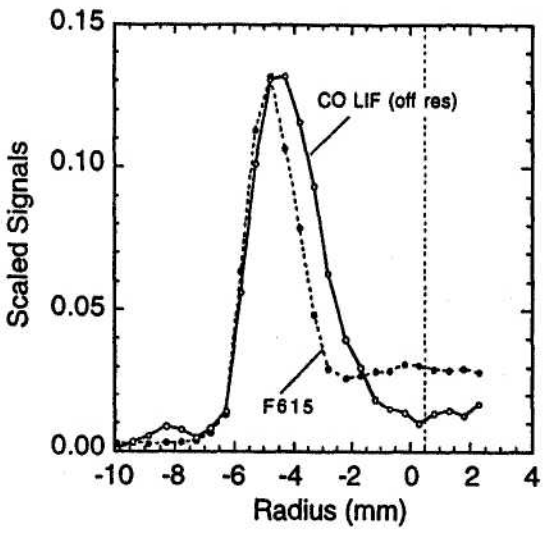

Fig. 11. Radial profiles of the averaged F615 signal and the averaged off-resonance CO-LIF signal in the laminar methane-air jet flame. Peak values have been matched to compare shapes. The F615 signal near the jet centerline includes a contribution from CH_4 Raman scattering.

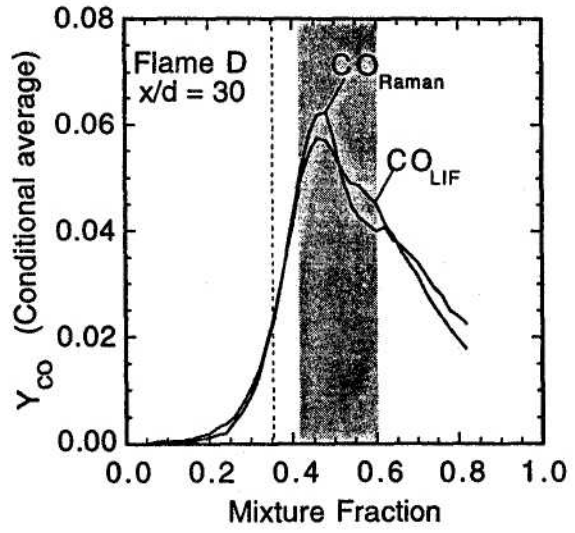

Fig. 12. Conditional mean CO mass fractions from Raman and LIF measurements in a piloted, turbulent jet flame of air-diluted methane. The shaded region indicates the mixture fraction interval where hydrocarbon fluorescence interferences are important.

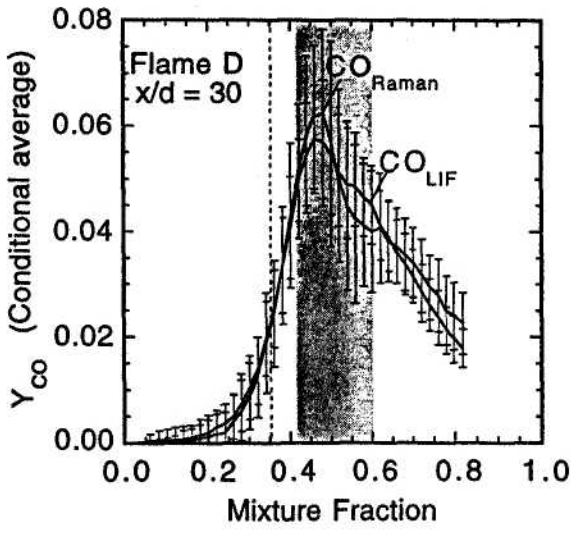

Fig. 13. Conditional rms fluctuations in the CO--Raman and CO-LIF results are plotted as uncertainty bars ($\pm\sigma$), with the LIF method yielding the smaller fluctuations.

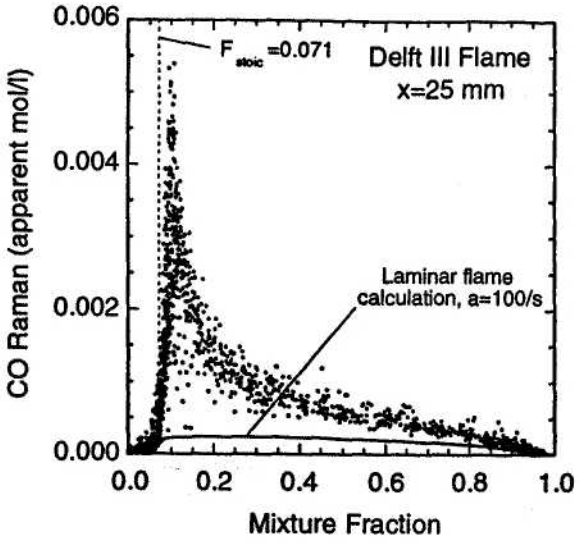

Fig. 14. Apparent CO concentrations from Raman measurements in the piloted natural gas flame before the application of the correction for hydrocarbon fluorescence interference. Results are compared to a laminar flame calculation.

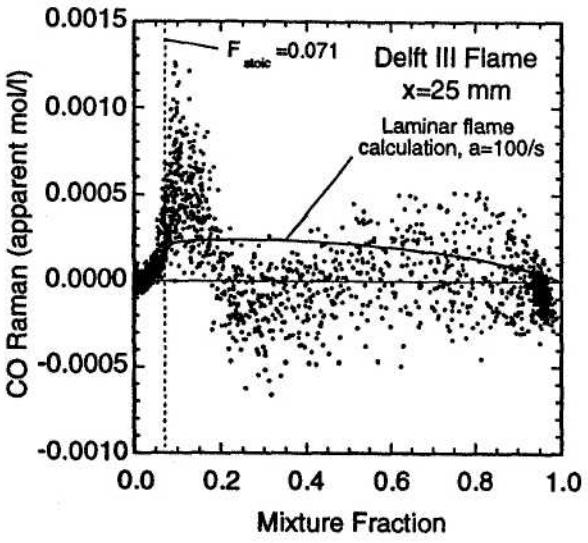

Fig. 15. Apparent concentrations after the correction is applied to the Raman measurements.

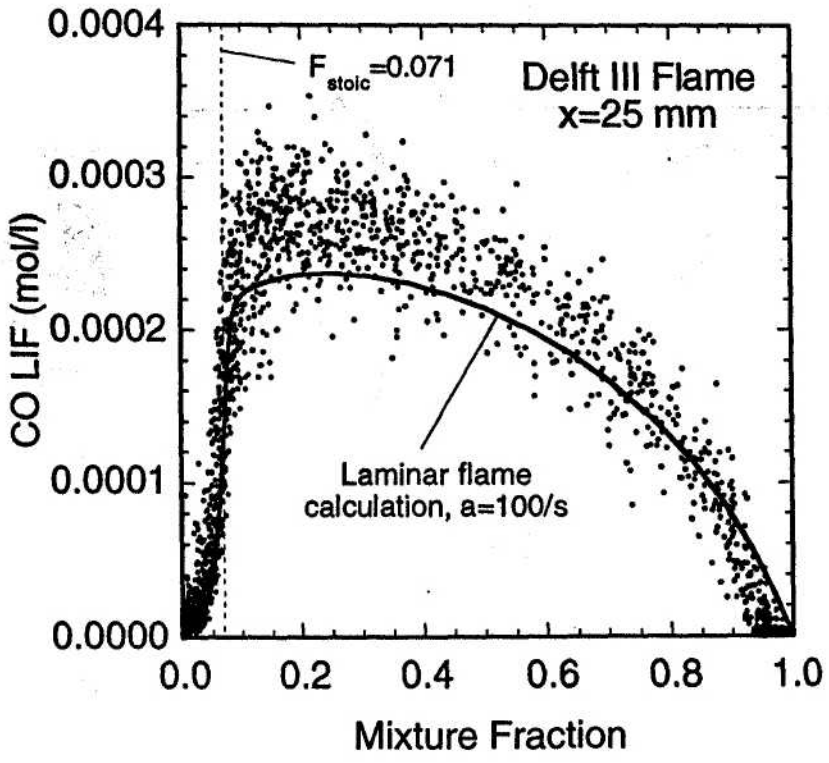

Fig. 16. CO concentrations from LIF measurements performed simultaneously with the Raman measurements shown in Fig. 14. The same laminar flame calculation is included.